

# Transition-Tempered Metadynamics Is a Promising Tool for Studying the Permeation of Drug-like Molecules through Membranes

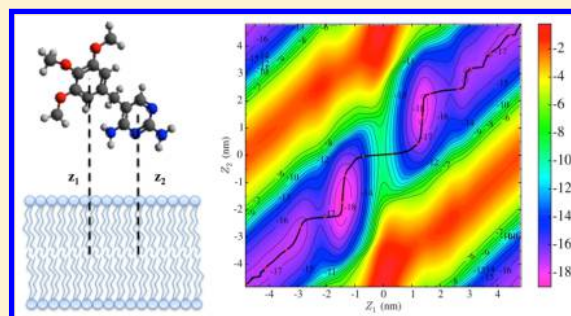
Rui Sun,<sup>†</sup> James F. Dama,<sup>†</sup> Jeffrey S. Tan,<sup>‡</sup> John P. Rose,<sup>‡</sup> and Gregory A. Voth<sup>\*,†</sup>

<sup>†</sup>Department of Chemistry, Institute for Biophysical Dynamics, James Franck Institute, and Computation Institute, The University of Chicago, 5735 South Ellis Avenue, Chicago, Illinois 60637, United States

<sup>‡</sup>Small Molecule Design & Development, Lilly Corporate Center, Eli Lilly & Company, Indianapolis, Indiana 46285, United States

**S** Supporting Information

**ABSTRACT:** Metadynamics is an important enhanced sampling technique in molecular dynamics simulation to efficiently explore potential energy surfaces. The recently developed transition-tempered metadynamics (TTMetaD) has been proven to converge asymptotically without sacrificing exploration of the collective variable space in the early stages of simulations, unlike other convergent metadynamics (MetaD) methods. We have applied TTMetaD to study the permeation of drug-like molecules through a lipid bilayer to further investigate the usefulness of this method as applied to problems of relevance to medicinal chemistry. First, ethanol permeation through a lipid bilayer was studied to compare TTMetaD with nontempered metadynamics and well-tempered metadynamics. The bias energies computed from various metadynamics simulations were compared to the potential of mean force calculated from umbrella sampling. Though all of the MetaD simulations agree with one another asymptotically, TTMetaD is able to predict the most accurate and reliable estimate of the potential of mean force in the early stages of the simulations and is robust to the choice of required additional parameters. We also show that using multiple randomly initialized replicas allows convergence analysis and also provides an efficient means to converge the simulations in shorter wall times and, more unexpectedly, in shorter CPU times; splitting the CPU time between multiple replicas appears to lead to less overall error. After validating the method, we studied the permeation of a more complicated drug-like molecule, trimethoprim. Three sets of TTMetaD simulations with different choices of collective variables were carried out, and all converged within feasible simulation time. The minimum free energy paths showed that TTMetaD was able to predict almost identical permeation mechanisms in each case despite significantly different definitions of collective variables.



## I. INTRODUCTION

Using molecular dynamics (MD) simulations with accurate force fields to study the physical and chemical processes of biological systems at atomistic resolution has seen great success over the last few decades.<sup>1</sup> However, due to the finite limitations on computational resources, a typical all-atom MD simulation can access at most the microsecond time scale for a system of a few hundreds of thousands of atoms.<sup>2</sup> Unfortunately, many biomolecular events such as folding and conformational transitions in proteins may take place on a much longer time scale in biological systems. Therefore, a large variety of enhanced sampling methods have been proposed to address this time scale issue.<sup>3,4</sup>

Metadynamics (MetaD) is one example of an enhanced sampling technique.<sup>5–7</sup> In MetaD, one chooses a set of appropriate collective variables (CVs),  $s$ , prior to simulation. Then, during simulation, the dynamics is accelerated by a history dependent bias potential  $V(s)$  that is built up sequentially.  $V(s)$  has the form of a summation of Gaussian functions centered at previously visited points, and it helps the chemical system to overcome large free energy barriers by discouraging it from

revisiting configurations that have already been sampled. After a long simulation, the bias potential makes every point equally likely to be sampled, offsetting the potential of mean force, and therefore the negative of the MetaD bias potential can be used to estimate the true underlying potential of mean force  $F(s)$ . In contrast with the advantages above, there are two major disadvantages. Firstly, instead of converging the bias potential to the actual potential of mean force, the bias potential oscillates around it. Eventually, the bias potential overfills all basins on the potential of mean force and pushes the system to high-energy regions on the collective variable space. Secondly, it can be very difficult to select appropriate collective variables among all degrees of freedom in the system.

To address the first disadvantage, the heights of the Gaussian functions that are added to the bias potential need to taper to zero as the bias potential grows across the collective variable space. The first implementation of this approach is well-tempered metadynamics (WTMetaD),<sup>8</sup> in which the Gaussian

Received: February 25, 2016

Published: September 6, 2016

heights decrease exponentially as a function of the bias potential on the collective variable space. The bias potentials computed from WTMetaD have been proven to converge to the inverse of the underlying potential of mean force asymptotically.<sup>9</sup> However, there is an obvious drawback that the decrease of the Gaussian height does not depend on whether the system has overcome the barriers between basins or not. This means that one is forced to make trade-offs between the computational resources spent until the first barrier crossing and the asymptotic convergence rate.

Choosing the appropriate bias factor, which controls the speed at which the Gaussian heights decrease, is far from trivial.<sup>10</sup> As the original WTMetaD paper showed,<sup>8</sup> as well as later in our TTMetaD paper,<sup>11</sup> the bias factor significantly affects WTMetaD convergence speed. In spite of its apparent success in many biochemical simulations, this sensitivity to the bias factor leads to two undesirable possibilities. On one hand, there is a possibility of false convergence when each increment of bias potential tapers too rapidly. In this case the bias potential does not appear to evolve in longer simulations, but it is in fact not converged. On the other hand, as pointed out in refs 10–12, WTMetaD that tapers the height of the Gaussian function too slowly sacrifices quality of its convergence. Instead of searching for a barrier height, there are many situations where it is much easier to estimate the positions of the basins in the CV space. An incomplete list of examples is as follows:

1. Permeation: basins could be easily chosen as the center of the permeation barrier (e.g., membrane interior) and the center of the bulk solvent (e.g., membrane exterior).
2. Protein Folding: basins could be easily chosen according to alpha-beta similarity and/or RMSF.
3. Thermodynamic Integration (TI) calculation: basins can be chosen as the end points of the TI.

The transition-tempered metadynamics (TTMetaD)<sup>11</sup> was recently developed to solve this problem in the cases that the rough basin locations can be identified. In TTMetaD, positions of basins are defined on the collective variable space prior to simulation, and the maximally biased path among all paths connecting the basins is used to exponentially temper the height of Gaussian functions. As a result, TTMetaD does not start tempering the height of Gaussians until the basins are relatively full and then aggressively tempers the Gaussian height to smoothly converge asymptotically. With this approach, TTMetaD is able to explore the collective variable space as efficiently as nontempered MetaD in the early stages of simulation and also is very robust to the choice of bias factor.

In this paper we performed TTMetaD simulations of the permeation of drug-like molecules through lipid bilayers. Small molecule permeation is involved in mass and signal transfers between the interior of a cell and its environment and is a fundamental process in almost every biological system. Even during the origins of life, building blocks of biopolymers and nutrients must have been able to passively permeate through the membrane to support primordial metabolism and cellular reproduction in the absence of protein transporters.<sup>13</sup> The permeation of small molecules is also essential in the drug delivery process, because this process is directly related to the ability of a given drug to penetrate into the cell interior, and therefore it serves as an important guide to how delivery kinetics and drug distribution can be selectively manipulated through candidate selection or chemical modification, administration route, etc.<sup>14</sup> Theoretically, the permeability coefficient can be computed from an atomistic simulation-based potential of mean force (PMF), via the inhomogeneous solubility diffusion model

$$\frac{1}{P} = \int_{z_2}^{z_1} \frac{dz}{D(z)} \exp[\beta F(z)] \quad (1)$$

in which  $F(z)$  is the PMF,  $D(z)$  is the local diffusion coefficient, and  $z$  is the position along the direction normal to the lipid bilayer.<sup>15,16</sup> The computation of the local diffusion coefficient  $D(z)$  has recently been reviewed elsewhere.<sup>17–19</sup>

In this work, we performed TTMetaD to compute the PMFs,  $F(z)$ , of the permeation processes for two small molecules through lipid bilayers. A recently published paper by Lee et al.<sup>20</sup> investigated the computation of  $F(z)$  by using umbrella sampling, replica exchange umbrella sampling, adaptive biasing force, and multiple-walker adaptive biasing and found no definitive advantage for any of these methods in their ability to predict the membrane permeability coefficient. The center of mass distance between the permeating molecule and membrane is used as the only CV in Lee's work.<sup>20</sup> Boicchio et al.<sup>10</sup> have compared the performance of umbrella sampling and metadynamics (nontempered MetaD and WTMetaD) for the calculation of free-energy landscapes composed of polyethylene and polypropylene oligomers interacting with lipid. Their research demonstrated that metadynamics and umbrella sampling yield the same estimates for the water-membrane free energy profile, but metadynamics can be more efficient, providing lower statistical uncertainties within the same simulation time. However, in the interest of completeness, although it is unclear that canonical umbrella sampling is more reliable than MetaD, we also computed PMFs from umbrella sampling as a reference against which to compare.

We employed permeation of ethanol through a 1-palmitoyl-2-oleoyl-*sn*-glycero-3-phosphocholine (POPC) lipid bilayer as our benchmark system to compare the performance of TTMetaD with nontempered MetaD and WTMetaD. We initiated multiple TTMetaD calculations from different randomly sampled initial states (configurations and velocities) and showed that the biases in these calculations converged almost exactly to the negative of the underlying PMF. We also showed that the average of the bias potentials from multiple TTMetaD simulation replicas converge much faster than an individual calculation. In addition to providing a check of the convergence of TTMetaD calculations, these calculations suggest that this approach can be more efficient in terms of simulation wall time. After verifying the performance of TTMetaD with the ethanol permeation system, we applied this method to the permeation of a more complicated drug-like molecule, trimethoprim. Despite the size and flexibility of trimethoprim, TTMetaD nonetheless yielded a convincingly converged PMF within a feasible simulation time. We further tested the robustness of the choice of CVs in TTMetaD and found that different choices of CVs induced negligible divergence of the permeation mechanisms from one another.

## II. METHODS

**2.1. Transition-Tempered Metadynamics.** In MetaD, an external history-dependent bias potential is added to the Hamiltonian of the system. The bias potential is a function of preselected CVs that putatively represent the important chemical dynamical processes of the system and is usually written in the form of a sum of Gaussians deposited throughout the simulations.<sup>6,7</sup> Therefore, the system is discouraged from revisiting configurations that have already been sampled on the CV space.

In nontempered MetaD, the bias potential  $V_G$  is set to be zero at the beginning of the simulation and evolves according to the equation

$$V_G(s, t) = \int_0^t dt' w \exp \left[ - \sum_{i=1}^d f(S_i(R)) \right] \quad (2)$$

in which  $w$  is the bias energy addition rate, usually expressed as the height of Gaussian function  $w_0$  divided by a deposition stride  $\tau$ . Each CV,  $S_i(R)$ , is a function of atomic coordinates of the system, and  $f(S_i(R))$  is defined as

$$f(S_i(R)) = \frac{(S_i(R) - S_i(R(t')))^2}{2\sigma_i^2} \quad (3)$$

where  $\sigma_i$  is the width of the Gaussian for the  $i^{\text{th}}$  CV. The history-dependent bias potential computed from nontempered MetaD does not converge modulo a constant but rather fluctuates around the desired final state.<sup>21,22</sup> WTMetaD was developed to address this problem by sequentially rescaling the height of Gaussians according to the bias potential that has already been added at that particular point in the CV space<sup>8,9</sup> according to the equation

$$w(t) = w_0 \exp \left[ - \frac{V_G(s, t)}{k_B \Delta T} \right] \quad (4)$$

in which  $\Delta T$  is a parameter chosen before calculation and tunes the rate of decrease in the Gaussian height. A bias factor,  $\gamma$ , is defined from  $\Delta T$  and the temperature ( $T$ ) of the system by

$$\gamma = \frac{T + \Delta T}{T} \quad (5)$$

As discussed previously in the paper, WTMetaD requires a choice between efficient exploration of the CV space at early stages of the calculation and the asymptotic convergence rate. On one hand, WTMetaD with a large  $\gamma$  will build up a fast-growing but noisy bias potential, hindering convergence. On the other hand, a small  $\gamma$  might prevent WTMetaD from escaping a minimum in a feasible simulation time, especially when at least one barrier in the CV space is very large, also delaying convergence.

TTMetaD is a method that smoothly converges like WTMetaD but avoids the trade-off between early exploration and asymptotic convergence rate.<sup>11</sup> The height of the Gaussian in TTMetaD is tempered as

$$w(t) = w_0 \exp \left[ - \frac{V^*(s(\lambda), t)}{k_B \Delta T} \right] \quad (6)$$

where  $V^*(s, t)$  is the minimal bias on the maximally biased path among all the continuous paths  $s(\lambda)$  that connects all of a set of preselected basin points on the CV space. A more intuitive description is that TTMetaD keeps track of the region in the CV space where the bias potential has explored and does not start decreasing the Gaussian height until all the basin points are included in this region and then progressively shrinks the hills as the region becomes better connected. Instead of the preknowledge of the barrier height required to choose the optimized  $\gamma$  for WTMetaD, only a rough guess of the basin points in the CV space is needed for TTMetaD.

The method for estimating PMFs from the nontempered MetaD bias potential trajectory follows previous work by Ghaemi et al.<sup>23</sup> The PMF was estimated as the time average of the bias

potential starting from the time when the dynamics becomes diffusive in CV space.<sup>24,25</sup> A rigorously optimal definition of the initial averaging time can be ambiguous and is beyond the scope of this paper; therefore, we averaged from both an aggressively early time, 30 ns (suggested in ref 23), and a conservatively late time, 200 ns. The estimated PMF for TTMetaD and nontempered MetaD is the inverse of the bias potential. For WTMetaD,<sup>8</sup> the PMF is instead estimated as

$$G(s) = \frac{\gamma}{1 - \gamma} V_G(s, t) \quad (7)$$

where  $\gamma$  is the bias factor defined in eq 5.

**2.2. Molecular Dynamics.** As noted earlier, we first tested the TTMetaD method on the permeation of ethanol through a POPC lipid bilayer and then applied TTMetaD to a more complicated molecule, trimethoprim, examining its permeation through the same lipid bilayer. The MD simulations were carried out using GROMACS-5.0.4<sup>26,27</sup> patched with PLUMED2<sup>28</sup> modified by the Voth research group<sup>11,12</sup> to perform TTMetaD using McGovern–de Pablo boundary conditions for all non-periodic CVs.<sup>29</sup> The lipid bilayer was made up of  $16 \times 2$  POPC molecules with the size inspired by the work of Ghaemi et al.<sup>23</sup> The bilayer was placed in the  $x$ – $y$  plane and solvated by 2064 water molecules. The simulated system had dimensions of approximately  $3.2 \text{ nm} \times 3.2 \text{ nm} \times 8.5 \text{ nm}$ , with periodic boundary conditions enforced along all directions of Cartesian space. For both systems, CHARMM36<sup>30</sup> was used for the lipid, and CHARMM general force fields (CGenFF)<sup>31</sup> were used for the small molecules (ethanol and trimethoprim). As suggested by CHARMM36 and CGenFF, water molecules were modeled by TIP3P.<sup>32</sup> The initial structure of the POPC lipid bilayer was prepared using CHARMM-GUI membrane builder<sup>33</sup> and equilibrated for 100 ns in water. The thickness of the lipid bilayer and the area per headgroup were compared to the experimental value to confirm the bilayer has been equilibrated properly. Then the small molecules were randomly packed into the system using PACKMOL.<sup>34</sup> The lipid and the water plus small molecules were individually coupled to two 323 K heat baths using velocity rescaling with a stochastic term.<sup>35</sup> Pressure control was also applied by a Berendsen barostat<sup>36</sup> in which the box was rescaled every 5 ps. The cutoff distance for the short-range neighbor list was 12 Å and the neighbor list was updated every 40 steps. Fast smooth Particle-Mesh Ewald (SPME)<sup>37</sup> was used to compute the long-range electrostatic interaction. All hydrogen bonds were constrained by linear constraint solver (LINCS),<sup>38</sup> and the MD integration time step was 0.2 fs. The initial velocities were randomly sampled from a Boltzmann distribution with a temperature of 323 K. This temperature was chosen to be consistent with ref 23 for the ethanol permeation system. The same temperature was used for trimethoprim permeation for the purpose of comparison with the ethanol results.

**2.3. Collective Variables.** In MetaD, the history-dependent bias potential is deposited into a low dimensional (usually fewer than three dimensions) CV space. However, identifying an adequate set of CVs from numerous degrees of freedom in the chemical system can be far from trivial. A poor choice of CVs can lead to hysteresis in the bias potential and possibly prevent the calculation from converging.<sup>7,39</sup> The general problem of choosing CVs is discussed elsewhere.<sup>40,41,10,42,43</sup> However, the nature of the permeation process helps to constrain the choice of CVs for MetaD in this application. For example, if one wants to use two CVs to model the permeation of a small molecule

through lipid bilayers, at least one CV should describe the translation of the small molecule through the lipid bilayer and the other should be used to account for the internal degrees of freedom of the drug molecule, a particular interaction between the drug molecule and lipid head groups, etc. Therefore, for the ethanol permeation system two CVs were chosen: *a.* the *z* component distance (*z*) between the centers of mass of ethanol and the membrane and *b.* the orientation ( $\theta$ ) between the vector connecting the hydroxyl oxygen to its adjacent carbon and the normal vector of the lipid bilayer (both are depicted in Figure 1).

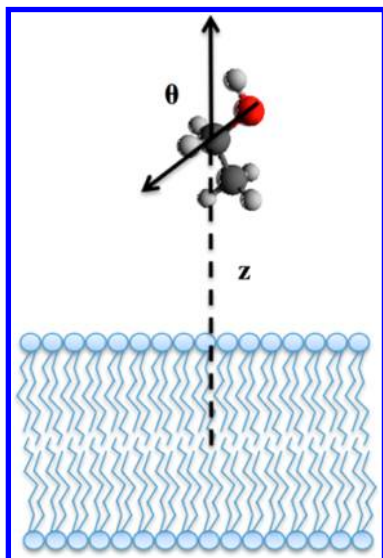


Figure 1. Definition of CVs for ethanol permeation.

Even though the purpose of this system is only to test the convergence of TTMetaD along the *z*-axis rather than investigate the permeation dynamics, the second CV ( $\theta$ ) will still be useful if one is interested in two questions:

1. What roles do the methyl and hydroxyl group play, when ethanol is near the surface between the bulk water and membrane?

2. Is there a certain alignment of ethanol preferred when it is in the membrane?

Since these problems have been addressed well elsewhere,<sup>44</sup> discussion about the dynamical role of the angle ( $\theta$ ) in our simulations is in qualitative agreement with it (results not shown). Robustness to the choice of CVs is also an important feature for an enhanced sampling method. It is especially important when applying a method to more complicated chemical systems in which identifying an optimal set of CVs is challenging. For the trimethoprim permeation system we defined three sets of CVs:

Set 1: CV1.1 = the *z* component distance between the centers of mass of trimethoprim and the membrane (*z*)

CV1.2 = the angle between the vector connecting the trimethoxybenzyl group to the pyrimidine group and the vector normal to the lipid bilayer ( $\theta$ )

Set 2: CV2.1 = the *z* component distance between the center of mass of the trimethoxybenzyl group and the membrane ( $z_1$ )

CV2.2 = the *z* component distance between the center of mass of the pyrimidine group and the membrane ( $z_2$ )

Set 3: CV3.1 = same as CV1.1 (*z*)

CV3.2 = the angle formed by the pyrimidine group center of mass, the center carbon atom, and the center of mass of the trimethoxybenzyl group ( $\Phi$ )

Those CVs are depicted in Figure 2. The first and second sets of CVs are chosen to investigate the orientation of trimethoprim during the permeation; therefore, TTMetaD should be able to converge both simulations to a similar effective permeation energy profile. In the third set of CVs, CV3.2 was deliberately chosen to be an angle bending term in the force field with a large restoring force; this set was designed to test the performance of TTMetaD when one of the CVs is not dynamically informative.

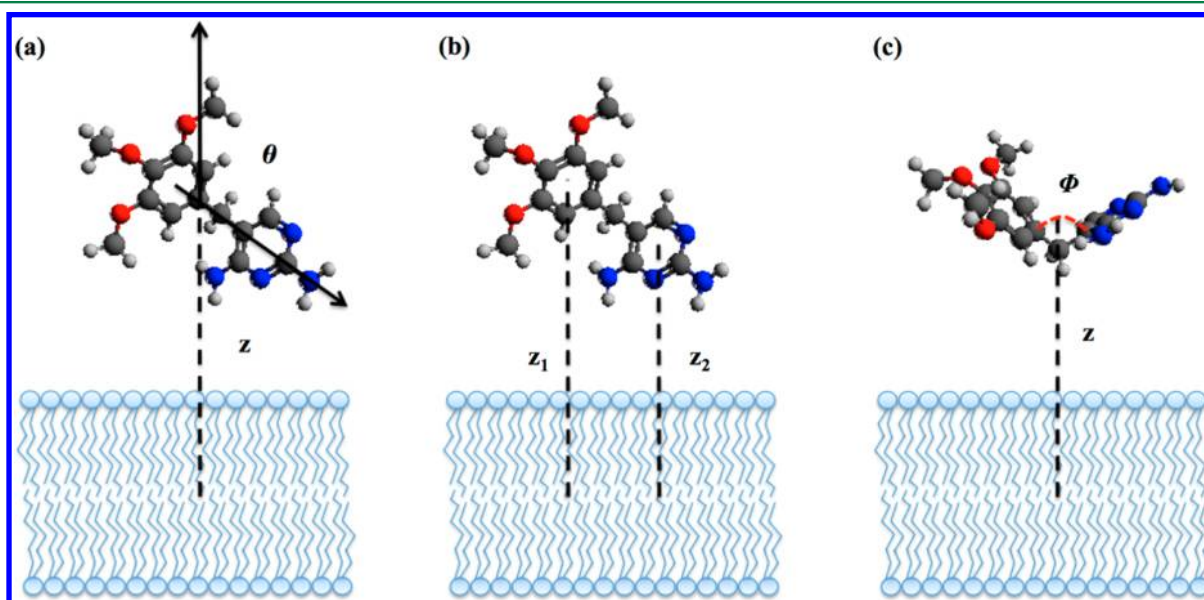


Figure 2. Definition of CVs for trimethoprim permeation. (a), (b), and (c) correspond to Set 1 (CV1.1 and CV1.2), Set 2 (CV2.1 and CV2.2), and Set 3 (CV3.1 and CV3.2), respectively.

### III. RESULTS AND DISCUSSION

**3.1. Ethanol Permeation through POPC Membrane.** To verify the advantages of TTMetaD, we first applied it to investigating the permeation of ethanol through POPC lipid bilayers and compared its performance with WTMetaD and nontempered MetaD. As discussed in the previous section, the two CVs were the  $z$  component distance,  $z$ , between the centers of mass of the ethanol and the membrane and the orientation, and  $\theta$ , between the vector connecting the hydroxyl oxygen to its adjacent carbon and the vector normal to the lipid bilayer. The same base Gaussian hill shape was used in TTMetaD, WTMetaD, and nontempered MetaD. The height of the Gaussian function was 0.02 kJ/mol, and the widths were 0.2 nm and 0.35 rad along the  $z$  and  $\theta$  directions, respectively. New Gaussian functions were added into the bias-potential once every picosecond in all simulations. These values were chosen in accordance with ref 23, where the same system was studied using nontempered bias-exchange metadynamics (BE-MetaD). Due to the intrinsic drawback of WTMetaD that there has to be a trade-off between the rate of exploration in early stages of simulation and the rate of asymptotic convergence, it required a significantly larger bias factor ( $\gamma = 11$ ) than was used in TTMetaD ( $\gamma = 5$ ). The two transition basins in TTMetaD were defined to be located at the center of the membrane and 1.3 nm away from the center of the membrane along the  $z$ -axis. The positions of the basins were estimated from the known thickness of the POPC lipid bilayers,<sup>30,45</sup> and therefore the primary permeation barrier in the CV space separates these wells.

Unfortunately, in more complicated systems this intuitive knowledge of the basin points might be very limited, making choosing meaningful positions for basins challenging. Thus, another set of TTMetaD calculations was performed where the basins were located 1.3 nm away from the center on each side of the lipid bilayer. This set of TTMetaD calculations will be denoted as TTMetaD(bad basins) from now on in the paper. These basin points were not well-chosen because the ethanol molecule is able to transit from one basin to the other through periodic boundaries instead of through the barrier (the lipid bilayer), which causes earlier tempering of the Gaussian height than desired. Due to these concerns about the positions of the basin points, a larger TTMetaD bias factor ( $\gamma = 8$ ) was employed for these TTMetaD calculations; we recommend using larger bias factors in this way whenever one may have chosen basin points that are not actually separated by the most important barriers. Using a larger bias factor is more conservative because when using a small bias factor the simulation may never cross the barriers and gives no information about them, whereas when using one that is too large one will still see barrier crossings and thereby be able to learn that the bias factor is too large.

A corresponding problem in WTMetaD is that the bias factor needs to be chosen according to the estimated barrier height, which is not always available. Therefore, another set of WTMetaD simulations with a smaller bias factor ( $\gamma = 7$ ) was also calculated to compare with the WTMetaD simulations with  $\gamma = 11$ . The purpose of these comparisons is to compare the robustness of TTMetaD and WTMetaD with respect to their input parameters (bias factor for WTMetaD; both bias factor and basin positions for TTMetaD). Seven independent replicas were calculated for 1  $\mu$ s for each TTMetaD, WTMetaD, and nontempered MetaD parameter set. In each replica, the ethanol molecule was placed into the solvent portion of the system randomly.

Due to the periodic boundary conditions and the homogeneity of lipid bilayer, a converged PMF should show symmetry with respect to the center of the membrane ( $z = 0$ ). Therefore, the maximum asymmetry  $V_G^{MA}(t)$  and average asymmetry  $V_G^{AA}(t)$  were introduced as criteria to show the quality of the convergence. They are chosen to measure convergence according to asymmetry and specific free energy differences, which do not depend on the standardization (average level) of the free energy surface. These were computed via

$$V_G^{MA}(t) = \max_z (|V_G(z, t) - V_G(-z, t)|) \quad (8)$$

$$V_G^{AA}(t) = \frac{\int dz |V_G(z, t) - V_G(-z, t)|}{\int dz} \quad (9)$$

The PMF from umbrella sampling<sup>46</sup> was calculated as a reference for MetaD energy estimates. A total of 51 umbrella windows, with distance between each of 0.01 (in the unit of box-scaled  $z$  value), were simulated for 60 ns each (10 ns equilibration plus 50 ns sampling). Therefore, only half of the permeation process PMF is actually sampled, and the other half is inferred as its reflected image with respect to the center of the membrane. A spring constant (3000 kJ/(mol/nm<sup>2</sup>)) was applied in each window. The weighted histogram analysis method (WHAM)<sup>47,48</sup> was employed to calculate the PMF from the set of independent histograms. The error bars on the 1D umbrella PMF range from 0.003 to 0.007 kcal/mol (51 umbrella windows), with an average value of 0.004 kcal/mol. The error bars were computed from the Monte Carlo bootstrap method for WHAM. To further verify this reference free energy, another simulation was performed on top of a frozen bias generated from TTMetaD after 1  $\mu$ s. The histogram of normalized  $z$  values (Supporting Information Figure S1) is nearly uniformly distributed in a 4-microsecond-long simulation. The frozen bias potential was then corrected to find a refined PMF via

$$V^{corr}(z, t) = -k_B T \log(h(z, t)) \quad (10)$$

where  $h(z, t)$  is the normalized probability of  $z$  in the simulation up to time  $t$ . This corrected bias estimator agrees very well with the PMF from umbrella sampling (Supporting Information Figure S2). As a measure of the error of bias potential along the simulation, we define the error as the root mean squared deviation from ref 8 such that

$$\varepsilon(t) = \left( \frac{1}{A} \int [V_G(z, t) - V^{ref}(z)]^2 dz \right)^{1/2} \quad (11)$$

in which  $V^{ref}$  is the reference PMF computed from umbrella sampling, and  $A$  is the integration area.

An umbrella sampling estimator<sup>49</sup> was used to estimate the PMF from metadynamics. Estimators make use of additional histogram information in addition to bias. The PMF is estimated via

$$V(z, t) = V_G(z, t) - k_B T \log(h(z, t)) \quad (12)$$

where  $V_G$  is the spontaneous bias potential, and  $h(z, t)$  is the normalized probability of  $z$  in the simulation up to time  $t$ . Unless otherwise noted, all the quantities reported in the manuscript are computed from the averaged PMF, which is defined as the following

$$\langle V_G(t) \rangle = \frac{1}{n} \sum_i^n V_G^i(t) \quad (13)$$

where  $i$  is the index of the individual replica, and  $n$  is the total number of replicas.

Figure 3 shows the averaged  $z$ -direction bias potential among seven walkers estimated from the bias potential in the early stages

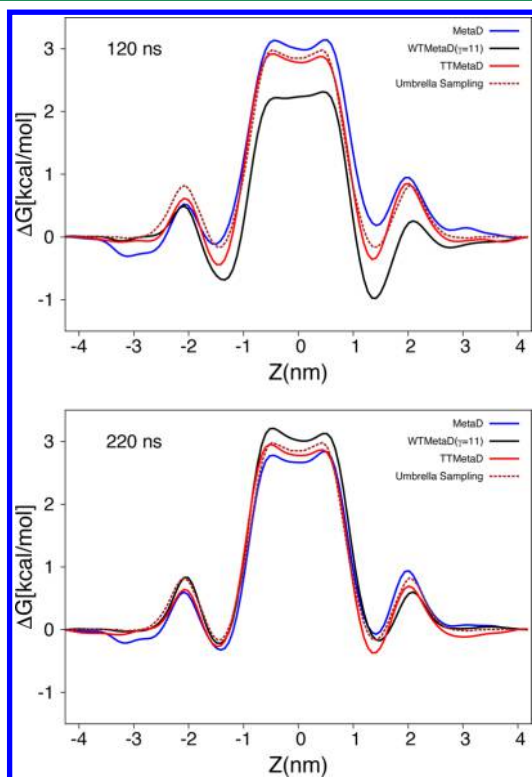


**Figure 3.** Free energy as a function of the position of ethanol in the  $z$ -direction normal to the membrane. The free energy was averaged over 7 random independent replicas for each method (eq 13).

of different MetaD simulations, when the bias potential has become qualitatively correct but not yet quantitatively accurate. At 120 ns (early stages of the simulation), the bias potential from TTMetaD lies between the PMF from nontempered MetaD and WTMetaD ( $\gamma = 11$ ), and it agrees notably better with the reference free energy from umbrella sampling. After another 100 ns (at 220 ns), the bias potential from WTMetaD ( $\gamma = 11$ ) increased significantly, and its agreement with the reference energy is approximately as good as the TTMetaD agreement. Successive refinement is expected from WTMetaD, as it has been proven to gradually converge. In contrast, this self-refining behavior is observed to a lesser extent in nontempered MetaD. As mentioned previously, we averaged the bias potential from nontempered MetaD starting from 30 ns (i.e., the 120 ns bias potential is the average of the bias from 30 to 120 ns), but in spite of this averaging, the agreement between the nontempered bias potential of 220 ns and the reference energy is only slightly better than that of 120 ns. As later figures show, the root mean squared deviations of nontempered MetaD PMF estimates from the reference actually increase with time at later times in our simulations.

The expected time of the first barrier-crossing event is an important quantitative measure of the efficiency of exploration of the CV space. In the present work, the first barrier-crossing event is defined as when ethanol transits from one side of the lipid bilayer to the other side through the membrane. Both the initial and final states of ethanol must be in the bulk water (instead of

local minima near the head groups of the lipid bilayer) and the transition must be through the lipid bilayer (instead of through the periodic boundaries). The full table of these times observed in our simulations can be found in the [Supporting Information](#). Although the TTMetaD, TTMetaD (bad basins), WTMetaD ( $\gamma = 11$ ), and nontempered MetaD all have different effective bias factors (5, 8, 11, infinity respectively), our results show statistically indistinguishable average first barrier crossing times: 57.9, 61.4, 51.4, and 39.3 ns respectively; statistical differences were estimated using the Mann–Whitney U test,<sup>50</sup> in which no two samples could be distinguished at the level  $P = 0.1$ . In contrast, WTMetaD ( $\gamma = 7$ ) with a bias factor of 7 showed a first barrier crossing time of 96.0 ns and was statistically significantly slower than both the nontempered MetaD ( $P = 0.062$ ) and the pooled escape times for all of the other indistinguishable methods ( $P = 0.054$ ) using the same Mann–Whitney test. The difference in average values confirms the trade-off between exploration and asymptotic convergence in WTMetaD and the relative insensitivity of this trade-off in TTMetaD with proper basins.

The estimated center barrier height was tracked throughout each of the microsecond long trajectories. It was defined as the free energy differences between two states: a. ethanol stays at the center of the membrane ( $z = 0$ ); b. ethanol stays in the headgroup region of membrane ( $z \approx 1.5$  nm). The average value of the center barrier height vs simulation time is shown in [Figure 4a](#). The center barrier height from each replica is shown in the [Supporting Information](#) (Figure S3). The center barrier height from all of the simulations converged to the same value asymptotically, except a small drift from nontempered MetaD in late stages of simulations. The time average of the bias potential starting averaging from 200 ns (Figure S4 in the [Supporting Information](#)) for nontempered MetaD behaves similarly to those starting averaging from 30 ns, confirming that aggressive initial average time recommended by Ghaemi et al.<sup>23</sup> is appropriate. The gold line marks the center barrier from an independent umbrella sampling reference, and the surrounding band denotes the range of 5% of its value (plus and minus 2.5%).

Our goal is to estimate the most important feature in the bias potential for the permeation process, the barrier height, to single-digit-percentage accuracy. A value of  $k_B T$  (0.64 kcal/mol, about 20% of the barrier height) has often been considered sufficient in earlier investigations, but in this paper we utilize a more precise standard. For example, we are interested in showing that MetaD is accurate enough to reveal any small differences between different force fields for comparison. The umbrella sampling estimator (eq 12), as pointed out in Branduardi et al.,<sup>49</sup> makes use of histogram information in addition to bias information and corrects for poorly chosen hill widths. [Figure 4b](#) illustrated the center barrier height from umbrella sampling estimator is close to the bias estimator, indicating our choice of hill width inherited from Ghaemi et al.<sup>23</sup> is appropriate and that including histogram information in the PMF estimator does not significantly affect the comparison between WTMetaD and TTMetaD in this case.

The properly set up TTMetaD example predicts an accurate central barrier height earliest, and both TTMetaD simulations were able to predict the center barrier height after 100 ns with relatively small fluctuations (compared to WTMetaD) afterward. WTMetaD ( $\gamma = 7$ ) touched the asymptotic center barrier height as quickly as TTMetaD but fluctuated more and with greater autocorrelation (see [Figure 4a](#) inset) afterward. The center barrier height from the other WTMetaD runs ( $\gamma = 11$ ) did not settle around the correct value until  $\sim 200$  ns and even then

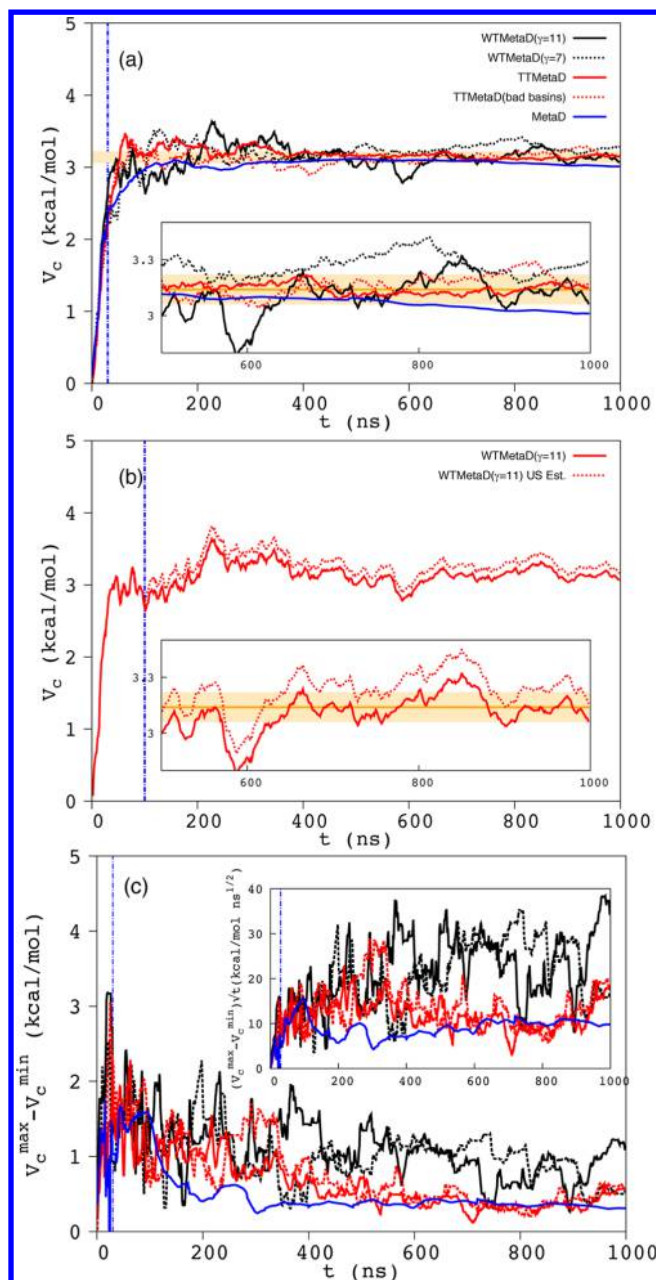


**Figure 4.** Panel (a): The center barrier height from nontempered MetaD averaged from 30 ns, WTMetaD and TTMetaD. Inset emphasizes the fluctuations seen at long times. The orange band identifies the range of 2.5% error from the umbrellas sampling center barrier height. Panel (b): The center barrier height from WTMetaD( $\gamma = 11$ ) and the umbrella sampling estimator, starting from 100 ns. Panel (c): the spread of the predicted center barrier from an ensemble of independent walkers,  $V_c^{\max}(t) - V_c^{\min}(t)$ . Inset illustrates the evolution of the same quantity multiplied by the square root of time to better illustrate asymptotic convergence.

continued to fluctuate far more than the other sets of runs—though with lower autocorrelation than the WTMetaD( $\gamma = 7$ ) set. The divergence between the two TTMetaD simulations is much smaller than that between the two WTMetaD simulations, showing the robustness of TTMetaD: even though the bias factors were different and the basin points in one simulation were defined as poorly as possible for this system, it still “healed” itself and converged relatively quickly.

As discussed previously, robust convergence cannot be confirmed until the PMF from each individual replica agrees with every other. Therefore, the differences between the maximum and minimum center barrier predicted from an ensemble of independent walkers,  $V_c^{\max}(t) - V_c^{\min}(t)$ , from each set of simulations are plotted in Figure 4c. This figure indicates how closely the PMFs predicted from each replica match one another.  $V_c^{\max}(t) - V_c^{\min}(t)$  from all the calculations decreased with longer simulation, indicating that each pair of replicas has become more similar in terms of bias potential at later times and further supporting the claim that these methods are in fact converging. A clearly different picture can be seen for the  $V_c^{\max}(t) - V_c^{\min}(t)$  from WTMetaD( $\gamma = 11$ ), which decreases more slowly than as in nontempered MetaD and TTMetaD. Combined with Figure 4a, it also shows TTMetaD is surprisingly robust to the choice of positions of the basin points, since both the solid and dashed red lines converge similarly.

This result may seem counterintuitive, since the higher the bias factor, the greater the expected long-time fluctuations of the bias. However, that intuition holds only for a single replica, and the average of the center barrier is a cross-replica quantity. In fact, across replicas, a too-early convergence in each individual replica causes early time sampling differences to lead to persistent differences between replicas even into late times. This too-early convergence is directly visible in the high autocorrelation seen in the WTMetaD( $\gamma = 7$ ) line of the top panel of Figure 4. Choosing a too-fast tempering rate slows down convergence even as it causes the illusion of convergence in individual replicas, a significant danger when using WTMetaD without replication. Importantly, the smaller  $V_c^{\max}(t) - V_c^{\min}(t)$  for TTMetaD indicates that individual replicas using TTMetaD are more reproducible than individual replicas from WTMetaD. This feature of TTMetaD is an essential advantage for simulations where multiple replicas are too expensive to carry out and therefore trustworthiness of individual runs is paramount.

The maximum asymmetry  $V_G^{MA}(t)$  was also checked along the course of the simulations, and the results are depicted in Figure 5a. To illustrate this, we only include the TTMetaD with the correct basin setup and WTMetaD with the better performance. As defined in eq 8, this quantity finds the most asymmetrically sampled point in the CV space by checking each point against its reflected image across the center of the membrane ( $z = 0$ ). This figure shows that the PMFs from TTMetaD and WTMetaD( $\gamma = 11$ ) converge to a similar asymmetry level asymptotically, while nontempered MetaD does not appear to converge.  $V_G^{MA}(t)$  decreases much more smoothly in TTMetaD than it does in WTMetaD( $\gamma = 11$ ), indicating that the bias has been fairly well converged in the early stages of the simulation and does not change dramatically at any region in the CV space afterward. Similar phenomena are found in Figure 5b for the average asymmetry.  $V_G^{AA}(t)$  from TTMetaD converges significantly more smoothly and is also slightly smaller, than that from WTMetaD( $\gamma = 11$ ). Nontempered MetaD, though it appears to predict the center barrier as well as TTMetaD, does not do as good a job of estimating the bias potential across the whole CV space. For example, the average asymmetry,  $V_G^{AA}(t)$ , for nontempered MetaD is more than two times larger than the value from TTMetaD after 1  $\mu$ s simulation. This asymmetry, presumably due to the fluctuating “bumpiness” of the bias potentials being averaged, but possibly also due to non-equilibrium effects of sustained high-energy driving, indicates relatively poor convergence. An illustration figure of the nontempered MetaD bias potential from each replica at the

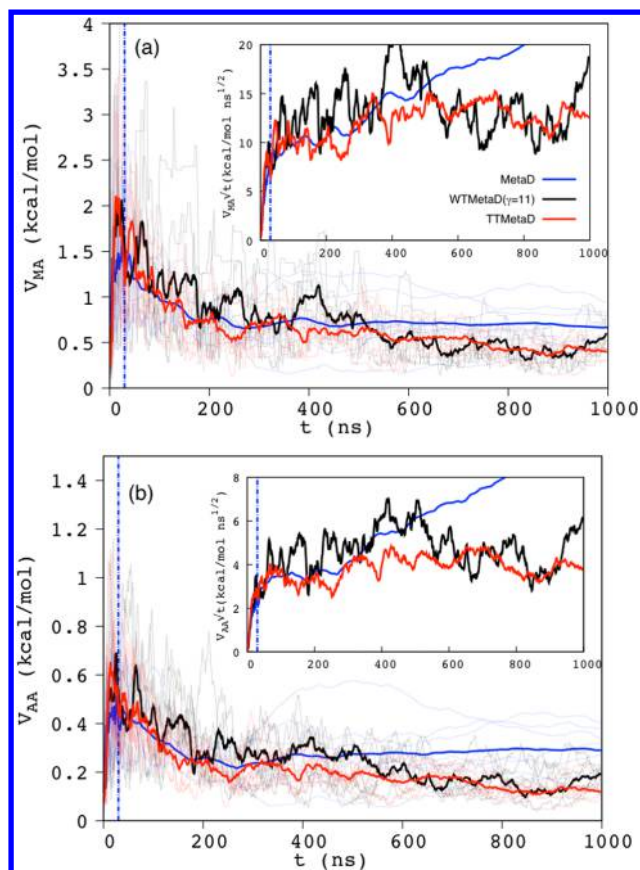


**Figure 5.** Panel (a): the maximum asymmetry from nontempered MetaD averaged from 30 ns, WTMetaD and TTMetaD. Panel (b): the average asymmetry with the same notation. The thin curves show the value from each individual replica and the bold curves are their averaged values. Inset illustrates the evolution of the same quantity multiplied by the square root of time, a typical error scaling for asymptotic convergence. Only the TTMetaD with the correct basin setup and WTMetaD with the better performance are shown.

end of the microsecond-long simulation is shown in Figure S5 in the Supporting Information. It is also noteworthy that  $V_G^{AA}(t)$  from nontempered MetaD becomes very stable after 500 ns, illustrating that it is not reaching the asymptotic convergence limit even with longer simulations. As a comparison,  $V_G^{AA}(t)$  from TTMetaD decreases approximately 40% from 500 to 1000 ns.

The total bias potential being added to the system increases as simulation time ( $t$ ) and its logarithm ( $\log(t)$ ) for nontempered MetaD and tempered MetaD (WTMetaD and TTMetaD), respectively. In tempered MetaD, the amount of energy being added to the system per period time decreases as  $1/t$ . Correspondingly,  $V_{MA}$  and  $V_{AA}$  change progressively more slowly and may not appear to converge to the eye on a linear time plot. In spite of its slow evolution, however, the  $V_{MA}$  and  $V_{AA}$  decrease near-monotonically in TTMetaD, and to a lesser degree the same is true in WTMetaD ( $\gamma = 11$ ); it is not inconsistent with our data to expect those values to approach zero asymptotically in longer simulations. In particular, the insets of these figures show the error scaled by the square root of time to allow for easy comparison by eye against the hypothesis that the error is decreasing like the reciprocal of the square root of time, a typical asymptotic convergence pattern.

Figure 6a illustrates the time evolution of average error for various MetaD simulations as compared to the reference energy

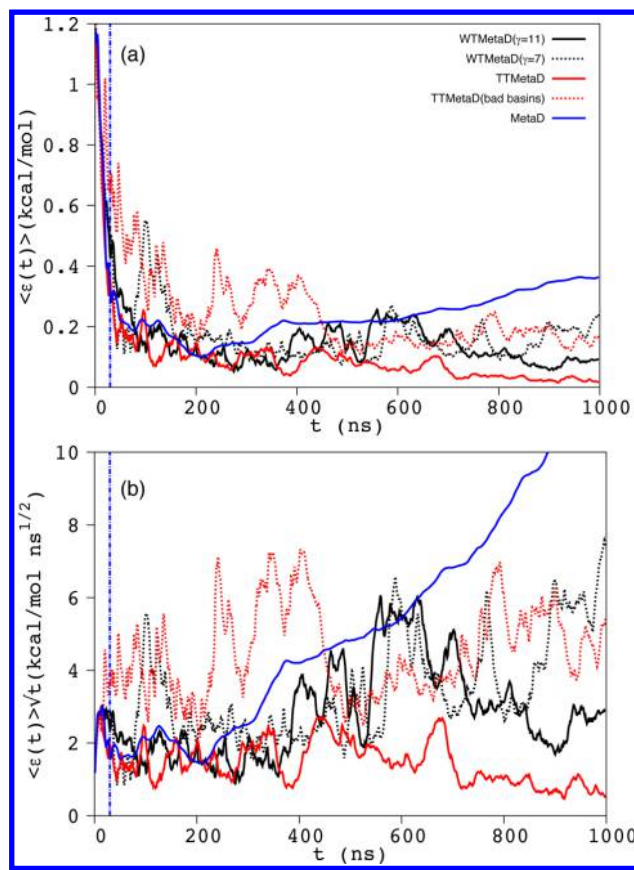


**Figure 6.** Panel (a): Time evolution of the error from averaged bias potentials (eq 13) for various MetaD simulations. Panel (b): Time evolution of error multiplied by square root of the simulation time. The error is defined in eq 11.

from umbrella sampling. The average errors from both WTMetaD and TTMetaD calculations decrease as the simulations go on. Appropriately designed TTMetaD converges almost exactly to the reference energy after 1  $\mu$ s, as does WTMetaD ( $\gamma = 11$ ) with slightly larger imprecision. It is also reasonable to expect, from Figure 6b, that the average error from TTMetaD converges to zero as  $1/\sqrt{t}$  after an initial transient period. WTMetaD ( $\gamma = 11$ ) behaves similarly with a longer autocorrelation time. Other tempered MetaD (TTMetaD-2(bas basins) and WTMetaD ( $\gamma = 7$ )) also appear to converge with diminishing fluctuations, though the fluctuation and autocorrelation of  $\epsilon(t)\sqrt{t}$  leaves this ambiguous.

However, in our nontempered MetaD simulations (averaging from 30 ns), it does not seem to converge to the reference PMF. Rather, it appears to show persistent error that grows nearly monotonically after 200 ns. The time evolution of the averaged bias potential from nontempered MetaD is depicted in the Supporting Information (Figure S6). The bias appears to have a persistent asymmetry just outside of the lipid headgroup region that cannot possibly correspond to the real PMF because the system is symmetric by construction. Though a small systematic error in nontempered MetaD could be expected; an error that grows with time is not. It could have been due to irregularities at the boundaries along the second collective variable, the theta angle, which is intrinsically bounded between 0 and  $\pi$ . Therefore, we carried out the same calculations with only one CV ( $z$ -coordinate). This drift does not appear in the 1D nontempered MetaD. A figure showing this via the average error along these

1D and 2D simulations is in the Supporting Information (Figure S8). This result implies that the variable theta, instead of nontempering MetaD, may indeed cause the small drift. With that being said, given the same collective variables, and with the same simulation time, the average error from tempered MetaD appears to be much more stable than nontempered MetaD.

In light of checking convergence from multiple independent replicas, it is clear that the PMF from averaging over these replicas dramatically increases the quality of the convergence at any stage of the simulation. This is consistent with an interpretation that the effect of autocorrelation following early time errors may be the most significant source of error in tempered metadynamics at long times. An example of the TTMetaD simulations is shown in Figure 7. The averaged PMF is calculated from eq 13. As shown in the figure, the averaged PMF,  $\langle V_G(t) \rangle$ , showed a large degree of symmetry even at very early stages of the simulation (i.e., after 100 ns). Combined with the evolution of the center barrier height (Figures 4a and 4c), these results show that TTMetaD was able to provide a reasonably converged ethanol permeation PMF within 150 ns of simulation with 7 walkers. The averaged replicas approach appears to significantly improve the calculation in the following ways:

1. In a comparable CPU time, the averaged replicas approach (7 walkers  $\times$  140 ns/walker) provides a more converged PMF than a single long replica simulation of the same length (980 ns).
2. In a comparable CPU time, the averaged replicas approach is much more efficient than a single long simulation in wall time because each walker can be run in parallel. Because of the independence of each replica, there is no overhead cost for this parallelization.
3. The averaged walkers approach provides intuitive on-the-fly checks of the quality of convergence.

**3.2. Trimethoprim Permeates through POPC Membrane.** Trimethoprim<sup>51</sup> (or 5-[(3,4,5-trimethoxyphenyl)-methyl]-2,4-pyrimidinediamine) is a commonly used antibacterial agent for treatment of acute otitis media, urinary tract infections, *Pneumocystis jiroveci* pneumonia, and travelers' diarrhea.<sup>52</sup> Trimethoprim is listed by the World Health Organization<sup>53</sup> as among the most important medications needed in a basic health system. Trimethoprim has a  $pK_a$  of 7.20,<sup>54</sup> and therefore it exists primarily as the neutral molecule in aqueous environments. After verifying the behavior of TTMetaD with a simple permeating molecule, ethanol, we then applied this method to trimethoprim, a much more complicated and pharmacologically relevant drug molecule.

As described previously, two CVs designed to investigate the orientation of the trimethoprim during the permeation process (CV1.1 and CV1.2) are defined as the distance ( $z$ ) between trimethoprim and lipid bilayer in the  $z$ -axis direction and the angle ( $\theta$ ) between the vector connecting the trimethoxybenzyl to the pyrimidine and the vector normal to the lipid bilayer (Figure 2a). We applied TTMetaD using these CVs with the positions of the basin defined in ( $z, \theta$ ) coordinates as (1.7 nm; 1 rad) and (0 nm; 2 rad), respectively. Averaging over multiple TTMetaD replicas was shown in the previous case to provide a well-converged PMF efficiently. Therefore, 5 replicas with randomized initial velocities and initial trimethoprim positions were calculated for this investigation. The predicted PMF after 1  $\mu$ s is shown in Figure 8, and the symmetry suggests good convergence of the TTMetaD calculations. As shown in the figure, the permeation of trimethoprim is predicted to follow a "triple-flip" mechanism. Trimethoprim first interacts with the head groups

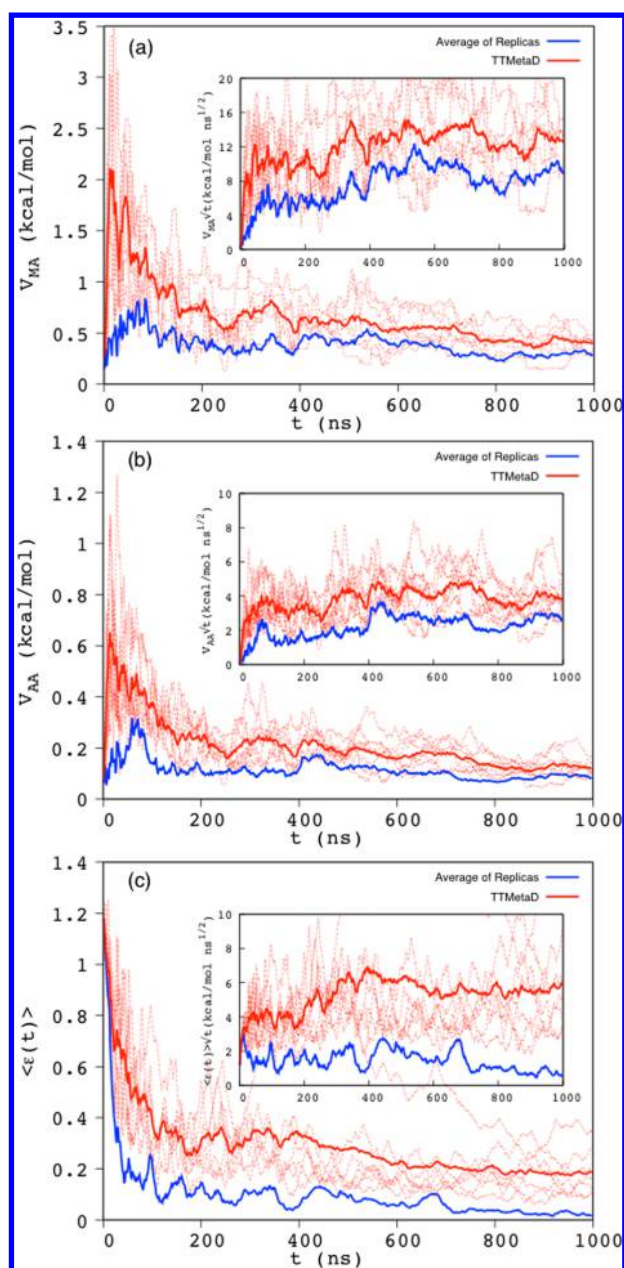


**Figure 7.** Comparison between averaged bias potential (eq 13) and individual replica in terms of (Panel (a)) the estimated maximum asymmetry ( $V_{MA}$ ), (Panel (b)) averaged asymmetry ( $V_{AA}$ ), and (Panel (c)) the RMSD error. The blue curves show the evolution of these quantities from the PMF obtained by averaging over replicas (eq 13). The thin red curves show the estimated values from each independent replica, and the bold red curves are their averaged values. Inset illustrates the evolution of the same quantity multiplied by the square root of time.

on one side of the lipid bilayers where there is a greater affinity between trimethoxybenzyl and the headgroup of membrane. When it starts to enter the membrane, the trimethoxybenzyl group preferentially stays in the headgroup region of the lipid, while the hydrophobic pyrimidine group flips into the region of lipid tails. Next, because of the hydrophobicity of the pyrimidine group, that end stays in the lipid tail region, while the trimethoxybenzyl group now flips with respect to the pyrimidine group for the trimethoprim to move to the other side of the lipid bilayer. Finally the pyrimidine flips out to the bulk water, while the trimethoxybenzyl group stays among the head groups,

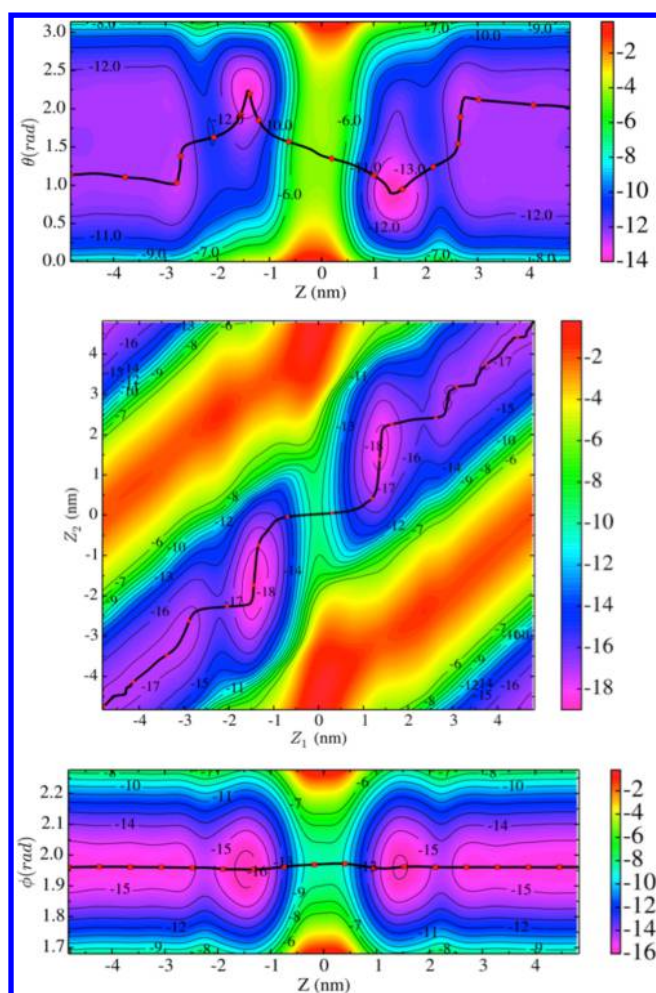


**Figure 8.** Potential of mean force in kcal/mol for the permeation of trimethoprim through the POPC bilayer. The top, middle, and bottom plots show the Set 1 (using CV1.1 and CV1.2), Set 2 (using CV2.1 and CV2.2), and Set 3 (using CV3.1 and CV3.2) of TTMetaD calculations, respectively. The definitions of those CVs are described in the text and shown in Figure 2. The unit of energy is kcal/mol. The black curves show the MFEP found from the string method.

finishing the permeation of the molecule from one side to the other. It is notable that the PMF is flat along  $\theta$  near  $z = 0$ , which indicates the interaction between trimethoxybenzyl group and headgroup of lipid is weak when trimethoprim is near the center of a lipid bilayer.

Another set of TTMetaD simulations was employed to confirm the PMFs found previously. As discussed in Section 2.3, the  $z$  component distances between the centers of mass of the trimethoxybenzyl ( $z_1$ ) and pyrimidine ( $z_2$ ) groups to the membrane were next used as the CVs to propagate TTMetaD (CV2.1 and CV2.2, see Figure 2b). In this case the positions of the TTMetaD basins were defined as (1.7 nm; 1.7 nm) and (0 nm; 0 nm). The same number of randomly initialized TTMetaD replicas as in the first set was simulated for 1  $\mu$ s and was averaged in the same manner as the first set. The resulting PMF is shown in the middle panel of Figure 7. The “triple-flip” mechanism is even clearer in this plot. The alignment between the two basins (near the center of the figure) and the  $Z_2$  axis indicates the flip of the pyrimidine group (first and third flip in the headgroup region of lipid), and the symmetry with respect to the center ( $z_1 = 0$ ;  $z_2 = 0$ ) indicates the flip of the trimethoxybenzyl group (second flip in

the tail group region of lipid). The two discrete basins at the top left and bottom right corners of the PMFs correspond to the states where trimethoprim is in bulk water. As compared to the first set of CVs, it is noteworthy that the second set of TTMetaD simulations should not be kept running too long because the bias potential will eventually try to push the trimethoxybenzyl group away from the pyrimidine group, possibly leading to numerical errors in the simulation.

Unfortunately, good intuitive preknowledge of the relevant systems might not be available for all the phenomena that one is interested in, and therefore it is of interest to test the robustness of the choice of CVs in TTMetaD simulations. The third set of CVs (CV3.1 and CV3.2, see Figure 2c) was designed for this purpose. The positions of the basins were defined as (1.7 nm; 1.7 rad) and (0 nm; 2.3 rad). It is well-known that the angle of C–C–C is very rigid, and therefore bending of the angle is expected to suffer large resistance due to the force field parameters. To be consistent with the previous simulations, five random TTMetaD replicas were simulated using these new CVs, and each replica ran 1  $\mu$ s. The averaged PMF is shown in Figure 8. The PMFs show that the permeation happens with the C–C–C bending angle staying very close to its minimum energy value throughout, though it is interesting to see that the range of the bending shrinks in the tail group region of the lipid bilayer. Judging by the previous two TTMetaD calculations, trimethoprim does not have a preferred orientation in this region, so the narrower range in the bending angle may come from the tail group region being more structuring as compared to bulk water.

If those simulations were properly converged and the CVs captured similar barriers, one would expect to obtain a similar minimum free energy path (MFEP) for the permeation process. The string method at zero temperature<sup>55</sup> was employed to search for the MFEP on the predicted PMFs, and the results are plotted as the black lines in Figure 8. The method proceeds by evolving strings, i.e., smooth curves with intrinsic parametrization whose dynamics takes them to the most probable transition path between two metastable regions in configuration space.<sup>56</sup> The MFEP was also projected onto the string length reaction coordinate, and the resulting one dimension plot is shown in Figure 9. In spite of the intentionally poor choice of CVs (CV3.2), the third set of TTMetaD simulations predicted almost an identical MFEP as the second set of TTMetaD simulations

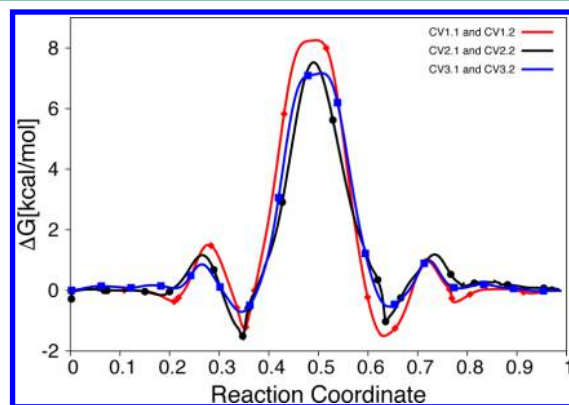


**Figure 9.** MFEP from three sets of TTMetaD calculations. The free energy of trimethoprim in bulk water has been set to zero. The reaction coordinate represents the permeation process. For example, 0 and 1 correspond trimethoprim to be in bulk water on different sides of the lipid bilayer. The red diamonds, black dots, and blue squares correspond to the same shape of marks in Figure 8.

(CV2.1 and CV2.2). The MFEP from the first set of TTMetaD calculations (using CV1.1 and CV1.2) agrees well with the other two sets of calculations except the center barrier region, where the former is about 10% larger. Notably, the MFEP from the first TTMetaD shows the worst symmetry with respect to its center among all three calculations, which indicates this calculation probably has not converged as well as the other two within the same amount of simulation time. The agreement would be expected to get better with longer simulation time. Overall, the MFEPs from different TTMetaD calculations are accurate enough to reveal differences along the MFEP of the different choices of CVs.

#### IV. CONCLUSIONS

Recently, TTMetaD has been developed by Dama et al.<sup>11</sup> to explore CV space efficiently at the early stages of a MetaD simulation without slowing down its asymptotic convergence. Compared to nontempered MetaD and WTMetaD, the parameters for TTMetaD are intended to be more robust. In this paper, TTMetaD was applied to study the permeation of small molecules through a lipid bilayer, an important subject in biochemistry and pharmaceutical science. The first permeating molecule studied in this paper was ethanol. The performance of nontempered MetaD, WTMetaD, and TTMetaD was compared, and the results showed the following:

1. Both WTMetaD and TTMetaD converged to the same PMF asymptotically and quantitatively match the reference free energy computed from umbrella sampling.
2. The PMFs estimated via TTMetaD in the earliest stages of simulation were superior to corresponding estimates from both WTMetaD and nontempered MetaD.
3. At later times TTMetaD performed similarly to the corresponding WTMetaD when basins were chosen as poorly as possible but outperformed WTMetaD in terms of retrospective error, symmetry, and reproducibility when the basins were chosen reasonably.
4. Nontempered MetaD did not converge spontaneously but nonetheless provided a reasonable estimate of PMF with time averaging until approximately 250 ns, after which instabilities appeared to arise.

Multiple replicates with randomly selected initial conditions were simulated to check the convergence, and analysis of the results of those simulations shows that the averaging over replicas estimates accurate bias potentials and the PMF more quickly in wall clock time. Remarkably, for all methods using multiple independent replicas leads to less error than using serial simulations of equal length in CPU time, suggesting that the dominant error in tempered metadynamics for this system is false convergence or long-persistent autocorrelation rather than fast random asymptotic fluctuation error. This multiple replica approach could be applied to relatively small systems to reach the true asymptotic convergence regime or to relatively large systems to get rough, qualitative convergence within a limited simulation wall time. Another benefit of using multiple replicas is the ability to check the convergence across the calculations to indicate a reasonable point to stop the simulation.

Trimethoprim was the other permeating molecule studied in this paper. Trimethoprim is made up of trimethoxybenzyl and pyrimidine groups that each has many internal degrees of freedom. The calculations suggested a “triple-flip” mechanism for the permeation: the first flip corresponds to the trimethoxybenzyl group staying in the headgroup region of lipids, while the pyrimidine group flips from bulk water into the tail group region

of the lipids. Due to the affinity between the trimethoxybenzyl group and the head groups of the lipids, trimethoprim flips again (second flip) with respect to the pyrimidine group when the trimethoxybenzyl group moves to the other side of the lipid bilayer. Finally, just as in the first flip except reversed, the pyrimidine group must flip out to the bulk water, while the trimethoxybenzyl group stays associated with the phospholipid head groups, finishing the permeation process. Another set of TTMetaD calculations carried out with a different, similar set of CVs confirmed this mechanism. Finally, we intentionally chose a deficient set of CVs to test the robustness of TTMetaD.

In addition to all of the advantages summarized above, TTMetaD is an enhanced sampling technique that is easy to understand and apply. TTMetaD has been implemented in a publicly available fork of the latest version of PLUMED2 and so is free to use. The extra input parameters that TTMetaD requires have robust defaults and are straightforward to incorporate into the input file, requiring only a line or two extra compared to a normal PLUMED2 run. Detailed information can be found in a user manual provided freely upon request. With existing technology any group already using MetaD and PLUMED2 can begin using TTMetaD simply by reinstalling PLUMED2 with any compatible MD engine.

#### ■ ASSOCIATED CONTENT

##### Supporting Information

The Supporting Information is available free of charge on the ACS Publications website at DOI: 10.1021/acs.jctc.6b00206.

Table showing the first center barrier-crossing times observed in simulations (Table S1); the histogram of the normalized  $z$  values from unbiased simulation on a bias from TTMetaD (Figure S1); the TTMetaD bias potential after 1 microsecond, corrected TTMetaD bias potential, and the reference energy from umbrella sampling (Figure S2); center barrier height from various MetaD simulations (Figure S3); comparisons of center barrier height and its spread between nontempered MetaD, WTMetaD, and TTMetaD, with nontempered MetaD averaged from 200 ns (Figure S4); bias potential from non-tempered MetaD as a function of the position of ethanol in the  $z$  direction normal to the membrane at 1000 ns (Figure S5); time evolution of bias potential from non-tempered MetaD (Figure S6); CV values in the last 50 ns of TTMetaD simulation (Figure S7); time evolution of the error from averaged bias potentials (Equation 13) for 1D and 2D MetaD simulations (Figure S8) (PDF)

#### ■ AUTHOR INFORMATION

##### Corresponding Author

\*E-mail: [gavoth@uchicago.edu](mailto:gavoth@uchicago.edu).

##### Author Contributions

R.S. and J.F.D. contributed equally.

##### Notes

The authors declare no competing financial interest.

#### ■ ACKNOWLEDGMENTS

This research was supported in part by the Eli Lilly and Company and in part by the National Science Foundation (NSF Grant CHE-1465248). Simulations were performed in part using resources provided by the University of Chicago Research Computing Center (RCC) and the San Diego Supercomputing Center (Comet) through the Extreme Science and Engineering

Discovery Environment (XSEDE), which is supported by the National Science Foundation grant number ACI-1053575.

## REFERENCES

- (1) Dror, R. O.; Dirks, R. M.; Grossman, J. P.; Xu, H.; Shaw, D. E. Biomolecular Simulation: A Computational Microscope for Molecular Biology. *Annu. Rev. Biophys.* **2012**, *41*, 429–452.
- (2) Saunders, M. G.; Voth, G. A. Coarse-Graining Methods for Computational Biology. *Annu. Rev. Biophys.* **2013**, *42*, 73–93.
- (3) Pohorille, A.; Jarzynski, C.; Chipot, C. Good Practices in Free-Energy Calculations. *J. Phys. Chem. B* **2010**, *114*, 10235–10253.
- (4) Schlick, T. Molecular Dynamics-Based Approaches for Enhanced Sampling of Long-Time, Large-Scale Conformational Changes in Biomolecules. *F1000 Bio. Rep.* **2009**, *1*, 51.
- (5) Laio, A.; Parrinello, M. Escaping Free-Energy Minima. *Proc. Natl. Acad. Sci. U. S. A.* **2002**, *99*, 12562–12566.
- (6) Sutto, L.; Marsili, S.; Gervasio, F. L. New Advances in Metadynamics. *Wires Comput. Mol. Sci.* **2012**, *2*, 771–779.
- (7) Barducci, A.; Bonomi, M.; Parrinello, M. Metadynamics. *Wires Comput. Mol. Sci.* **2011**, *1*, 826–843.
- (8) Barducci, A.; Bussi, G.; Parrinello, M. Well-Tempered Metadynamics: A Smoothly Converging and Tunable Free-Energy Method. *Phys. Rev. Lett.* **2008**, *100*, 020603.
- (9) Dama, J. F.; Parrinello, M.; Voth, G. A. Well-Tempered Metadynamics Converges Asymptotically. *Phys. Rev. Lett.* **2014**, *112*, 240602.
- (10) Bochicchio, D.; Panizon, E.; Ferrando, R.; Monticelli, L.; Rossi, G. Calculating the Free Energy of Transfer of Small Solutes into a Model Lipid Membrane: Comparison between Metadynamics and Umbrella Sampling. *J. Chem. Phys.* **2015**, *143*, 144108.
- (11) Dama, J. F.; Rotskoff, G.; Parrinello, M.; Voth, G. A. Transition-Tempered Metadynamics: Robust, Convergent Metadynamics Via on-the-Fly Transition Barrier Estimation. *J. Chem. Theory Comput.* **2014**, *10*, 3626–3633.
- (12) Dama, J. F.; Hocky, G. M.; Sun, R.; Voth, G. A. Exploring Valleys without Climbing Every Peak: More Efficient and Forgiving Metabasin Metadynamics Via Robust on-the-Fly Bias Domain Restriction. *J. Chem. Theory Comput.* **2015**, *11*, 5638.
- (13) Wei, C. Y.; Pohorille, A. Permeation of Membranes by Ribose and Its Diastereomers. *J. Am. Chem. Soc.* **2009**, *131*, 10237–10245.
- (14) Xiang, T. X.; Anderson, B. D. Liposomal Drug Transport: A Molecular Perspective from Molecular Dynamics Simulations in Lipid Bilayers. *Adv. Drug Delivery Rev.* **2006**, *58*, 1357–1378.
- (15) Marrink, S. J.; Berendsen, H. J. C. Simulation of Water Transport through a Lipid-Membrane. *J. Phys. Chem.* **1994**, *98*, 4155–4168.
- (16) Marrink, S. J.; Berendsen, H. J. C. Permeation Process of Small Molecules across Lipid Membranes Studied by Molecular Dynamics Simulations. *J. Phys. Chem.* **1996**, *100*, 16729–16738.
- (17) Comer, J.; Chipot, C.; Gonzalez-Nilo, F. D. Calculating Position-Dependent Diffusivity in Biased Molecular Dynamics Simulations. *J. Chem. Theory Comput.* **2013**, *9*, 876–882.
- (18) Basconi, J. E.; Shirts, M. R. Effects of Temperature Control Algorithms on Transport Properties and Kinetics in Molecular Dynamics Simulations. *J. Chem. Theory Comput.* **2013**, *9*, 2887–2899.
- (19) Yeh, I. C.; Hummer, G. System-Size Dependence of Diffusion Coefficients and Viscosities from Molecular Dynamics Simulations with Periodic Boundary Conditions. *J. Phys. Chem. B* **2004**, *108*, 15873–15879.
- (20) Lee, C. T.; Comer, J.; Herndon, C.; Leung, N.; Pavlova, A.; Swift, R. V.; Tung, C.; Rowley, C. N.; Amaro, R. E.; Chipot, C.; Wang, Y.; Gumbart, J. C. Simulation-Based Approaches for Determining Membrane Permeability of Small Compounds. *J. Chem. Inf. Model.* **2016**, *56*, 721–733.
- (21) Laio, A.; Rodriguez-Forteza, A.; Gervasio, F. L.; Ceccarelli, M.; Parrinello, M. Assessing the Accuracy of Metadynamics. *J. Phys. Chem. B* **2005**, *109*, 6714–21.
- (22) Bussi, G.; Laio, A.; Parrinello, M. Equilibrium Free Energies from Nonequilibrium Metadynamics. *Phys. Rev. Lett.* **2006**, *96*, 090601.
- (23) Ghaemi, Z.; Minozzi, M.; Carloni, P.; Laio, A. A Novel Approach to the Investigation of Passive Molecular Permeation through Lipid Bilayers from Atomistic Simulations. *J. Phys. Chem. B* **2012**, *116*, 8714–8721.
- (24) Crespo, Y.; Marinelli, F.; Pietrucci, F.; Laio, A. Metadynamics Convergence Law in a Multidimensional System. *Phys. Rev. E* **2010**, *81*, 055701.
- (25) Laio, A.; Gervasio, F. L. Metadynamics: A Method to Simulate Rare Events and Reconstruct the Free Energy in Biophysics, Chemistry and Material Science. *Rep. Prog. Phys.* **2008**, *71*, 126601.
- (26) Berendsen, H. J. C.; Vandespoel, D.; Vandrunen, R. Gromacs - a Message-Passing Parallel Molecular-Dynamics Implementation. *Comput. Phys. Commun.* **1995**, *91*, 43–56.
- (27) Pronk, S.; Pall, S.; Schulz, R.; Larsson, P.; Bjelkmar, P.; Apostolov, R.; Shirts, M. R.; Smith, J. C.; Kasson, P. M.; van der Spoel, D.; Hess, B.; Lindahl, E. Gromacs 4.5: A High-Throughput and Highly Parallel Open Source Molecular Simulation Toolkit. *Bioinformatics* **2013**, *29*, 845–854.
- (28) Tribello, G. A.; Bonomi, M.; Branduardi, D.; Camilloni, C.; Bussi, G.; Tribello, G. A.; Bonomi, M.; Branduardi, D.; Camilloni, C.; Bussi, G. Plumed 2: New Feathers for an Old Bird. *Comput. Phys. Commun.* **2014**, *185*, 604–613.
- (29) McGovern, M.; de Pablo, J. A Boundary Correction Algorithm for Metadynamics in Multiple Dimensions. *J. Chem. Phys.* **2013**, *139*, 084102.
- (30) Klauda, J. B.; Venable, R. M.; Freites, J. A.; O'Connor, J. W.; Tobias, D. J.; Mondragon-Ramirez, C.; Vorobyov, I.; MacKerell, A. D., Jr.; Pastor, R. W. Update of the Charmm All-Atom Additive Force Field for Lipids: Validation on Six Lipid Types. *J. Phys. Chem. B* **2010**, *114*, 7830–43.
- (31) Vanommeslaeghe, K.; Hatcher, E.; Acharya, C.; Kundu, S.; Zhong, S.; Shim, J.; Darian, E.; Guvench, O.; Lopes, P.; Vorobyov, I.; MacKerell, A. D. CHARMM General Force Field (CGenFF): A Force Field for Drug-Like Molecules Compatible with the CHARMM All-Atom Additive Biological Force Fields. *J. Comput. Chem.* **2010**, *31*, 671–690.
- (32) Jorgensen, W. L.; Chandrasekhar, J.; Madura, J. D.; Impey, R. W.; Klein, M. L. Comparison of Simple Potential Functions for Simulating Liquid Water. *J. Chem. Phys.* **1983**, *79*, 926–935.
- (33) Jo, S.; Lim, J. B.; Klauda, J. B.; Im, W. CHARMM-GUI Membrane Builder for Mixed Bilayers and Its Application to Yeast Membranes. *Biophys. J.* **2009**, *97*, 50–58.
- (34) Martinez, L.; Andrade, R.; Birgin, E. G.; Martinez, J. M. Packmol: A Package for Building Initial Configurations for Molecular Dynamics Simulations. *J. Comput. Chem.* **2009**, *30*, 2157–2164.
- (35) Bussi, G.; Donadio, D.; Parrinello, M. Canonical Sampling through Velocity Rescaling. *J. Chem. Phys.* **2007**, *126*, 014101.
- (36) Berendsen, H. J. C.; Postma, J. P. M.; van Gunsteren, W. F.; DiNola, A.; Haak, J. R. Molecular Dynamics with Coupling to an External Bath. *J. Chem. Phys.* **1984**, *81*, 3684–3690.
- (37) Essmann, U.; Perera, L.; Berkowitz, M. L.; Darden, T.; Lee, H.; Pedersen, L. G.; Smooth, A. Particle Mesh Ewald Method. *J. Chem. Phys.* **1995**, *103*, 8577–8593.
- (38) Hess, B.; Bekker, H.; Berendsen, H. J.; Fraaije, J. G. Lincs: A Linear Constraint Solver for Molecular Simulations. *J. Comput. Chem.* **1997**, *18*, 1463–1472.
- (39) Dama, J. F.; Hocky, G. M.; Sun, R.; Voth, G. A. Exploring Valleys without Climbing Every Peak: More Efficient and Forgiving Metabasin Metadynamics Via Robust on-the-Fly Bias Domain Restriction. *J. Chem. Theory Comput.* **2015**, *11*, 5638–5650.
- (40) Berezhkovskii, A.; Szabo, A. Time Scale Separation Leads to Position-Dependent Diffusion Along a Slow Coordinate. *J. Chem. Phys.* **2011**, *135*, 074108.
- (41) Chen, M.; Yu, T.-Q.; Tuckerman, M. E. Locating Landmarks on High-Dimensional Free Energy Surfaces. *Proc. Natl. Acad. Sci. U. S. A.* **2015**, *112*, 3235–3240.
- (42) Ceriotti, M.; Tribello, G. A.; Parrinello, M. Simplifying the Representation of Complex Free-Energy Landscapes Using Sketch-Map. *Proc. Natl. Acad. Sci. U. S. A.* **2011**, *108*, 13023–13028.

- (43) Best, R. B.; Hummer, G. Reaction Coordinates and Rates from Transition Paths. *Proc. Natl. Acad. Sci. U. S. A.* **2005**, *102*, 6732–6737.
- (44) Comer, J.; Schulten, K.; Chipot, C. Diffusive Models of Membrane Permeation with Explicit Orientational Freedom. *J. Chem. Theory Comput.* **2014**, *10*, 2710–2718.
- (45) Tieleman, D. P.; Forrest, L. R.; Sansom, M. S. P.; Berendsen, H. J. C. Lipid Properties and the Orientation of Aromatic Residues in Ompf, Influenza M2, and Alamethicin Systems: Molecular Dynamics Simulations. *Biochemistry* **1998**, *37*, 17554–17561.
- (46) Torrie, G. M.; Valleau, J. P. Nonphysical Sampling Distributions in Monte Carlo Free-Energy Estimation: Umbrella Sampling. *J. Comput. Phys.* **1977**, *23*, 187–199.
- (47) Kumar, S.; Rosenberg, J. M.; Bouzida, D.; Swendsen, R. H.; Kollman, P. A. The Weighted Histogram Analysis Method for Free-Energy Calculations on Biomolecules. I. The Method. *J. Comput. Chem.* **1992**, *13*, 1011–1021.
- (48) Grossfield, A. Wham: The Weighted Histogram Analysis Method. version 2.0.9.
- (49) Branduardi, D.; Bussi, G.; Parrinello, M. Metadynamics with Adaptive Gaussians. *J. Chem. Theory Comput.* **2012**, *8*, 2247–2254.
- (50) Mann, H. B.; Whitney, D. R. On a Test of Whether One of Two Random Variables Is Stochastically Larger Than the Other. *Ann. Math. Stat.* **1947**, *18*, 50–60.
- (51) Darrell, J. H.; Garrod, L. P.; Waterworth, P. M. Trimethoprim: Laboratory and Clinical Studies. *J. Clin. Pathol.* **1968**, *21*, 202–209.
- (52) Eliopoulos, G. M.; Huovinen, P. Resistance to Trimethoprim-Sulfamethoxazole. *Clin. Infect. Dis.* **2001**, *32*, 1608–1614.
- (53) World Health Organization, Who Model List of Essential Medicines. 2015.
- (54) Perrin, D. D.; Dempsey, B.; Serjeant, E. P. Introduction. In *pKa Prediction for Organic Acids and Bases*; Springer: Netherlands, 1981; pp 1–11.
- (55) E, W.; Ren, W. Q.; Vanden-Eijnden, E. Finite Temperature String Method for the Study of Rare Events. *J. Phys. Chem. B* **2005**, *109*, 6688–6693.
- (56) E, W.; Ren, W.; Vanden-Eijnden, E. String Method for the Study of Rare Events. *Phys. Rev. B: Condens. Matter Mater. Phys.* **2002**, *66*, 052301.